LARS Information Note 110273

The Atmospheric Effect in Remote Sensing of Earth Surface Reflectivities

W. L. Murray and
G. M. Jurica

The Laboratory for Applications of Remote Sensing

Purdue University, West Lafayette, Indiana

1973

LARS Information Note 110273

THE ATMOSPHERIC EFFECT IN REMOTE SENSING OF EARTH SURFACE REFLECTIVITIES

by
W.L. Murray
and
G.M. Jurica

August 1973

TABLE OF CONTENTS

LIST OF FIGURES

ABSTRACT

This study represents a theoretical investigation of potential difficulties caused by the presence of the atmosphere in the identification of surface features by remote sensing techniques. Through interaction with atmospheric gaseous constituents and aerosol particles, a beam of radiant intensity will be affected by processes which can both increase and decrease its magnitude. The net effect of these intensity modifications, termed the "atmospheric effect," introduces an apparent change in the surface reflectivity which would be inferred from a measurement by an airborne sensing device pointed at a surface target. An erroneous surface classification may result.

Computations are performed using a series of computer programs which permit numerical evaluation of the intensity of scattered radiation at selected levels of a plane parallel, inhomogeneous atmosphere containing an arbitrary vertical distribution of ozone concentration and/or an aerosol number density, and bounded at the lower surface by a Lambert ground of known reflectivity. The basic technique used in solving the radiative transfer equation in this series of programs entails the expression of the

---

The work described in this report was funded by NASA under Grants NGL 15-005-112 and NAS5-21773.

scattering phase function by a Fourier series.

Results are computed for several realistic atmospheres when illuminated by radiation having a wavelength of 0.45 μm and of 0.70 μm. Aerosol populations considered are: no aerosol, a water droplet aerosol, and a silicate aerosol, the latter two having a discontinuous size distribution function with a maximum particle size of 10.0 μm. Results computed with an atmosphere included in the model are compared with results expected if the atmosphere had zero optical thickness, that is, no modifying effect. The atmosphere induced changes are then equated to equivalent surface reflectivity changes in a zero optical thickness situation.

These equivalent reflectivity changes are related to changes in solar zenith angle, altitude of observation, orientation of the plane of observation in relation to the plane of propagation, wavelength of incident radiation, and scattering characteristics of the included aerosol. Results are discussed for the following values of these parameters: solar zenith angles of 0°, 20°, and 40°; observation altitudes of 10,000 feet and 60,000 feet; azimuthal separation of the planes of observation and propagation of 0° and 90°; incident radiation with $\lambda = 0.45$ μm and $\lambda = 0.70$ μm; and aerosols with indices of refraction of $m = 1.33 - 0.00i$ and $m = 1.56 - 0.00i$. Underlying surface reflectivities of 0.10 and 0.15, corresponding to natural vegetation type surfaces, are used in the model when parameter changes are related to corresponding surface reflectivity changes. The maximum change noted is 0.1223.

1. INTRODUCTION

1.1 Surface Mapping: Why and How

In a topographical sense, the features of the earth's surface are well known. From the standpoint of earth resources, however, mapping of the terrestrial surface is by no means complete. Further geological studies of the composition of the surface are required in the search for petroleum, natural gas, coal, and the various minerals needed by our technological society.

Agriculture also has a definite need for improved knowledge of the characteristics of land surfaces. Such studies would help insure that the crops planted in a given area would be well suited to the soil type. Monitoring the stages of growth of existing vegetation would lead to early detection of diseased or blighted areas.

To conduct the required surveys of the earth's surface by actual on-site inspection can be extremely time consuming. A geologist or agronomist in the field might take weeks to map the characteristics of a relatively small area. On the other hand, a sensing device carried aboard an airplane or satellite might be able to inspect the same area in a matter of hours, or even minutes.

By conducting the surveys from the air, however, problems are

introduced. The most obvious is that the scientist no longer has direct physical contact with the subject of his examination. Research in the area of remote sensing has shown that this need not be an insurmountable problem. Through the use of a sensing device which measures the intensity of radiant energy emitted and reflected by a given surface at predetermined, discrete intervals of the electromagnetic spectrum, a great deal can be determined about the characteristics of that surface.

Since the physical and chemical properties of different surface types vary considerably, they have different spectral reflectance, or response, patterns. This spectral response pattern, or "signature," gives unique identifying characteristics to a surface in the form of the amount of visible radiation it reflects, and the temperature, hence wavelength, at which it emits infrared radiation. Remote sensing techniques can distinguish these "signatures" and thus identify various surface types. Therefore, accurate data combined with proper analysis techniques can yield the discriminations necessary to correctly map the characteristics of the surface.

The requirements for correct identification lead us to another problem connected with airborne or satellite-borne radiation sensing devices. The radiant energy does not pass unimpeded from the surface to the sensor. Instead, the signal undergoes modification due to the presence of the earth's atmosphere. This modification, sometimes called the atmospheric effect, may lead to erroneous surface classification if it is neglected. This study represents a theoretical examination of the importance of the atmospheric effect in the remote sensing problem.

1.2 The Atmospheric Effect

The atmosphere is composed primarily of nitrogen and oxygen, plus several trace gasses and suspended matter, or aerosols. As a beam of radiation passes through an atmospheric layer of finite optical thickness, the photons of radiant energy comprising the beam will interact with the gas molecules and larger suspended particles. These interactions, which are subject only to the conservation of energy, can result in a dual modification of the intensity of the radiant beam. In one sense, the atmosphere acts as a signal generator and increases the intensity; in another sense, the atmosphere acts as a filter and reduces the intensity. The resultant of these two modifying processes is the atmospheric effect.

The situation considered in this study relates to remote sensing and is based upon the use of a downward pointing, airborne sensor. Figure 1-1 illustrates several cases in which the atmosphere acts as a signal generator for this configuration.

drawing (a): illustrates a photon being scattered into the field of view of the sensor, after surface reflectance

drawing (b): illustrates a photon being scattered into the field of view of the sensor, prior to surface reflectance

drawing (c): illustrates a photon being emitted into the field of view of the sensor

Figure 1-2 illustrates several cases in which the atmosphere acts as a signal filter.

drawing (a): illustrates atmospheric absorption of a photon which is within the field of view of the sensor

drawing (b): illustrates a photon being scattered out of the field

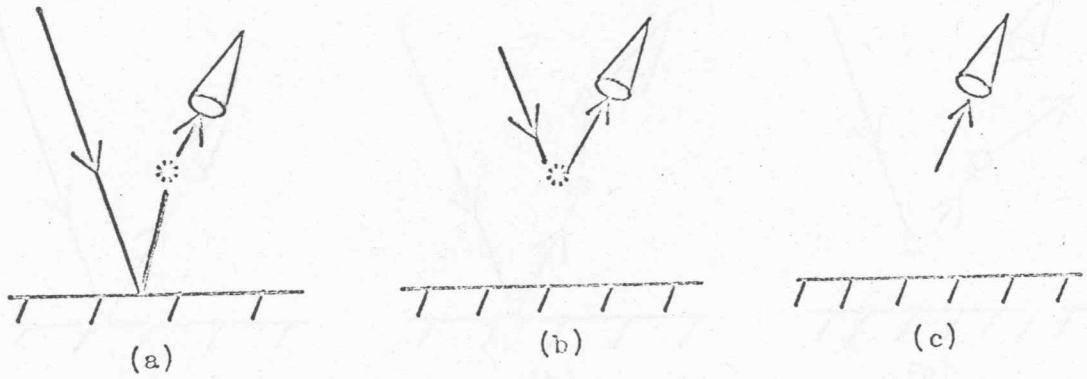

Figure 1-1 The Atmosphere as a Signal Generator

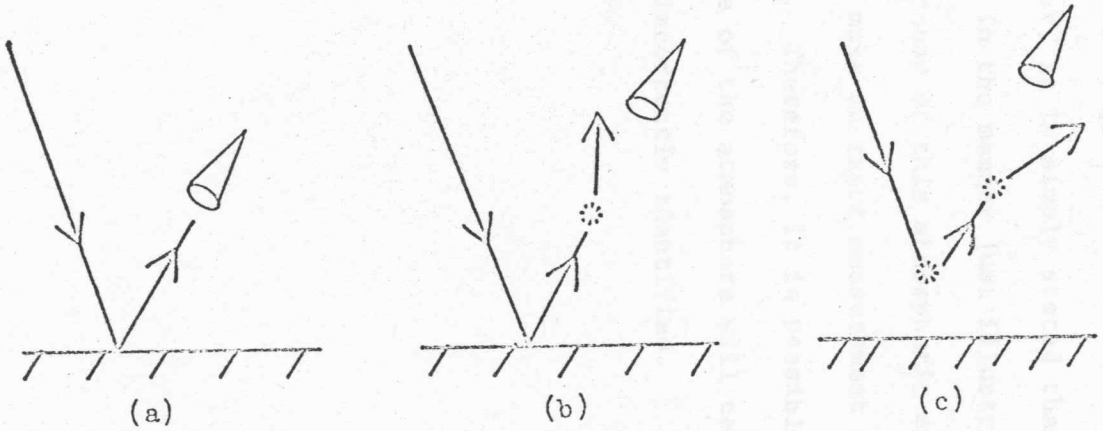

Figure 1-2 The Atmosphere as a Signal Filter

of view of the sensor, after surface reflectance

drawing (c): illustrates a photon being scattered out of the field of view of the sensor, prior to surface reflectance

A theoretical discussion of the scattering and absorption/emission processes will be given in the next chapter. For introductory purposes here, however, it is simply stated that they occur. Because they do occur and operate in the manner just illustrated, an atmospheric effect also exists. Because of this atmospheric effect, a sensor pointed at the surface cannot make an exact measurement of the radiant intensity leaving that target. Therefore, it is possible that the modifying effect due to the presence of the atmosphere will cause the sought after surface feature to be incorrectly identified.

2. LITERATURE SURVEY

2.1 Introduction

This study is concerned with the interaction between the beams of radiant energy which comprise a radiation field and the gaseous molecules and suspended particles which make up the earth's atmosphere. The computations described in later sections deal only with radiation in the visible portion of the electromagnetic spectrum. In presenting the basic problem, however, discussions will not be limited to this range. The theory is also pertinent to radiation in the infrared portion of the spectrum.

The fundamental principle governing the interaction of radiant energy and the components of the atmosphere is that energy must be conserved. This principle is stated mathematically in the radiative transfer equation, which is the mathematical tool used in quantitatively evaluating the atmospheric effect. The literature reviewed in this chapter covers the basic concepts required in the development of the radiative transfer equation. The equation, itself, will be formally presented in the next chapter.

2.2 The Principles of Radiative Transfer

A beam of radiant energy is composed of many photons. As a photon passes through the atmosphere, it may be subjected to any number of collisions with atmospheric molecules or suspended particles. Each collision may result in either the absorption of the photon or the scattering of the photon. Absorption is wavelength dependent and can be quantified in terms of an absorption coefficient based on the characteristics and concentration of the absorbing matter. Scattering, also, is a complicated process and a historical review of some highlights in the development of scattering theory is necessary to illustrate the depth of the problem.

Lord Rayleigh (1871) showed that when the radius of a scattering particle is much smaller than the wavelength of the incident radiation, the fraction of incident radiation scattered will be inversely proportional to the fourth power of the wavelength. Furthermore, the scattering pattern will be relatively symmetrical with forward and backward components equal and twice as large as the sideward components.

Rayleigh's approximation is quite satisfactory as a basis for studying molecular scattering of visible light. Atmospheric molecules have radii of less than 10Å while the wavelength of visible light ranges from 0.4 μm to 0.7 μm. However, the atmosphere frequently contains suspended particles, or aerosols, with radii of the same order as the wavelength of incident light. McClatchey, et al. (1972) suggest an upper size limit on the order of 10 μm. Here the Rayleigh approximation no longer applies.

When the particle size is of the order of, or somewhat larger than, the wavelength of the incident radiation, its scattering characteristics can be explained using the theory developed by Mie (1908). Mie's work

is based on Maxwell's electromagnetic field theory and represents the general development of radiation scattering principles of which Rayleigh's approximation is a special case. Mie, after applying appropriate boundary conditions, derived differential equations which describe the electromagnetic field at any point in space resulting from the illumination of an homogeneous spherical particle by a beam of radiation from any given direction. The assumption of an homogeneous and spherical particle is less than ideal, but it is closely approximated in nature by at least the water droplet aerosol. One very important characteristic of the Mie scattering process is that it shows a strong predominance of forward scattering with a secondary maximum in the backscattering region and a minimum near the side scattering direction.

Although the scattering properties of a single particle can be explained in terms of the Mie theory, a layer of atmosphere is composed of many particles. Thus the applications of scattering theory to actual atmospheric situations must consider the transfer of radiant energy through such a layer and not merely scattering due to a single particle. This problem was solved by Chandrasekhar (1950) when he achieved an exact solution to the problem of the transfer of radiant energy through an homogeneous plane-parallel atmosphere characterized by Rayleigh scattering. Chandrasekhar's solution of the theory of radiative transfer is nicely summarized in a paper by Sekera (1957) dealing with the state of the art of light scattering and radiative transfer in the mid-1950s.

The solution by Chandrasekhar also laid the groundwork for a set of tables by Coulson, Dave, and Sekera (1960) which give the exact emergent intensities of reflected and transmitted light in a Rayleigh type atmosphere. Other refinements in the theory of light scattering by small

particles were carried out by van de Hulst, and reported on in an excellent book (1957) on the subject. This work is very thorough for both single scattering particles and for populations of identical scattering particles.

As radiative transfer solution techniques became more refined it was possible to study situations more closely related to actual atmospheric conditions, particularly through the inclusion of the larger particles, or aerosols, in atmospheric models. This was done by Deirmendjian (1969) who compiled a monograph containing tables listing the scattering parameters characteristic of several polydispersions and aerosol compositions actually occurring in the terrestrial atmosphere. The term polydispersion refers to suspensions of particles of differing sizes.

Three basic techniques are currently being used to investigate the transfer of radiant energy in an actual scattering atmosphere. The first was developed by Herman and Browning (1965). This is the iterative technique and consists of repeatedly solving the radiative transfer equation at successive atmospheric levels and for all directions desired until a consistent set of intensities is obtained. This would yield the radiation field after one scattering process. Since multiple scattering is possible, these values then serve as the input for a repeat of the iterative process for second-order scattering. The computation is repeated for successively higher orders of scattering until sufficient accuracy is obtained.

The second technique was developed by Plass and Kattawar (1968) and is known as the Monte Carlo technique. This is a statistical process in which very great numbers of individual photons are forced to penetrate the scattering medium. Through an integration of the Mie scattering function over all space, a probability is determined for post-collision propagation

by the photon in any given direction. A probability value is also assigned to represent the likelihood of a collision resulting in absorption. Thus, all energy is accounted for and the path of travel through the attenuating medium can be predicted for an individual photon. For sufficiently numerous repeats of this process a statistically smooth radiation field will result.

The third technique is the Fourier series technique as developed by Dave (1970 A). This is a mathematical technique in which the scattering properties of a given attenuating medium can be predicted in terms of a Fourier series expansion. This is the method of solution of the radiative transfer equation used in this study and will be explained in detail in the next chapter.

3. COMPUTATIONAL PROCEDURES

3.1 Introduction

Computational procedures used in this study were developed under contract by J. V. Dave (1972) of the IBM Corporation for the National Aeronautics and Space Administration. In a series of four computer programs, an atmospheric model is developed which permits the user to compute the intensity of attenuated radiation at selected levels of a plane-parallel, nonhomogeneous atmosphere containing an arbitrary vertical distribution of an absorbent gas and/or an arbitrary aerosol population, and bounded at the lower surface by a Lambert ground of known reflectivity. The four programs are called Scalar Program A, Scalar Program B, Scalar Program C, and Scalar Program D. All programs were adapted to be run on an IBM 360 Model 67 computer.

3.2 SPA

This program is designed to compute the scattering characteristics of single spherical particles of a known index of refraction. As stated in the previous chapter, the size of the scattering particle is important in determining the resultant radiation field only in the sense of its ratio to the wavelength of the incident radiation. Consequently, computations are performed in terms of a dimensionless size parameter x which is defined by the relationship $x = \frac{2\pi r}{\lambda}$. The term r represents particle radius and λ is the wavelength of incident radiation. Since the program is run for monochromatic radiation λ is a fixed quantity, and selection of the proper range of values of x ensures that scattering properties will be computed for the desired particle sizes.

The input quantities to this program are the index of refraction of the particles being considered, the minimum value of x for which computations are required, an increment value of x for successive computations, and the number of times which x must be incremented.

Computations performed in SPA represent a solution to the basic Mie scattering problem, and utilize the following procedure. The values of the complex Mie amplitudes, which represent the components of the scattered radiation field perpendicular and parallel to the scattering plane are determined for each value of x (Deirmendjian, 1969, Chap. 2). Utilizing these Mie coefficients, efficiency factors for scattering and extinction and an asymmetry factor, $\overline{\cos\theta}$, are computed (van de Hulst, 1957, Chap. 9). The efficiency factors represent the ratios of the total amount of energy removed from the incident beam by scattering and by extinction to the geometric cross section of the particle. The asymmetry factor, in which $\bar{\theta}$ is the angle between the direction of the incident beam and the direction of

observation, introduces the directional nature of the scattering process into the problem.

Making use of these parameters, it is possible to determine the normalized scattering phase function. This function represents the fraction of incident radiant intensity which will be scattered into a particular direction when the scattering particle is illuminated by a beam coming from a given direction. The integral of the phase function over all directions thus equals unity. The scattering phase function can then be represented in terms of a Legendre series (Dave, 1970B).

The basic coefficients of the Legendre series computed in SPA then serve as input data to SPB in which the problem is expanded to account for attenuation by a unit volume containing a known size distribution of particles.

3.3 SPB

In this program, the scattering characteristics determined for single particles in SPA are applied to a situation in which a unit volume, containing a specified size distribution of spherical particles with a known index of refraction, is illuminated by unidirectional, monochromatic electromagnetic radiation. The program enables the user to compute a volume extinction coefficient, a volume scattering coefficient, a volume absorption coefficient, and a normalized scattering phase function for the unit volume.

The aerosol population considered in this study conforms to a discontinuous power law type distribution (Bullrich, 1964). This is characterized by a constant concentration of particles for equal increments of radius between the minimum radius considered, 0.03 μm, and an intermediate radius, 0.10 μm. Between 0.10 μm and the maximum size, 10 μm, particle concentration decreases with inverse proportionality to the fourth power of the radius.

To solve for the volume extinction, scattering, and absorption coefficients, the efficiency factors defined in SPA are integrated over the size range of particles present in the unit volume. The particle concentration function is included within the integral, and in this manner these quantities are properly weighted by the number of particles present in each size increment. Integrations are carried out using the trapezoidal rule with an integration increment of $\frac{\lambda \Delta x}{2\pi}$.

By an identical integration technique, the scattering phase functions determined for individual particles in SPA are modified to represent the directional scattering characteristics of the unit volume. The computed normalized scattering phase function for the unit volume is represented

by a Legendre series, with the coefficients serving as input values to SPC.

3.4 SPC

This program performs a dual function. First, the geometry is introduced which is most easily adapted to the computation of radiant intensities in a situation in which the earth is illuminated by energy from the sun. Secondly, mathematical manipulations are performed which incorporate the new geometry into the problem, and transform previously computed Legendre series representations of the scattering phase function into Fourier series form.

In programs SPA and SPB, scattering calculations have been carried out using the plane defined by the direction of incidence and the direction of scattering as a reference system. In actual practice it is preferable to use a reference system defined in terms of two vertical planes. The first plane contains the local vertical and the direction of incident solar radiation. The included angle between these two vector quantities is the solar zenith angle which is denoted θ_o . The second plane contains the local vertical and the direction of scattering. The included angle between these two quantities is the scattered radiation zenith angle, θ, which equals the look angle of the sensor, α, as seen in Figure 3-1. The construction of the new reference system is then completed with the introduction of azimuth angles ϕ and ϕ', which locate the planes containing θ and θ_o, respectively. In computations, ϕ' is assumed to be zero; that is, the plane containing the direction of propagation is the reference plane. The scattering angle, $\bar{\theta}$, is seen in Figure 3-1 to be the angle between the directions of propation of the incident and scattered intensities.

Finally, SPC performs the necessary mathematical steps to express the normalized scattering phase function of a unit volume in terms of a Fourier series whose argument is $\phi - \phi'$. This procedure is well documented

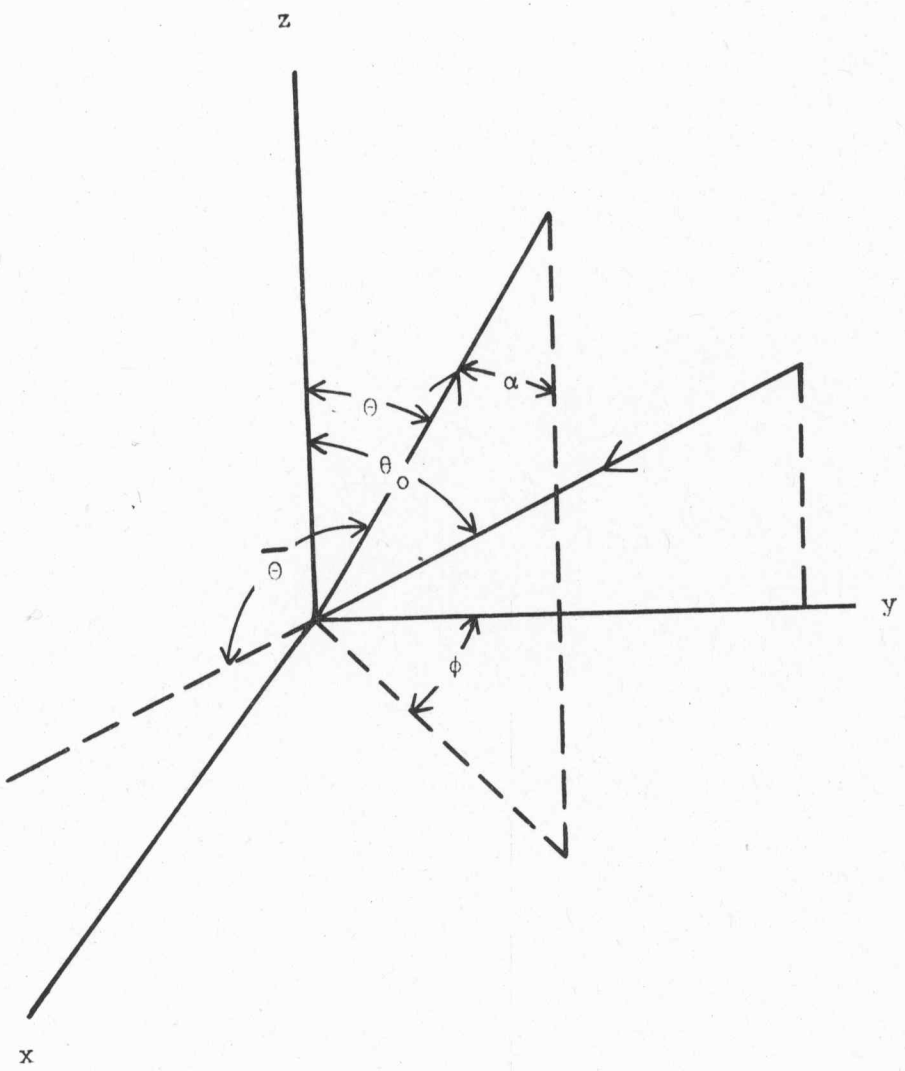

Figure 3-1 The Geometry of the Problem

(Dave and Gazdag, 1970; Dave, 1970A; Dave, 1970B), and represents the final prepatory step to achieving a solution to the radiative transfer equation in SPD.

3.5 SPD

This program solves the radiative transfer equation when an atmosphere of known composition, with an underlying Lambertian surface of specified reflectivity, is illuminated by parallel beam radiation coming from a source with a known zenith angle. A theoretical discussion of the radiative transfer equation is required to illustrate the physical principles applied in achieving this solution.

3.5.1 The Radiative Transfer Equation

The intensity, I_λ, of a beam of monochromatic radiant energy, contained within a solid angle $d\omega$, passing through a volume element of area dA and thickness ds is subject to both a positive change and a negative change due to interaction with the matter contained within the unit volume.

Energy may be removed from the direction of propagation of I_λ through either absorption or scattering. The sum of these two processes is called attenuation and can be expressed mathematically as

$$-k_{\lambda t}\rho I_\lambda ds dA d\omega$$

where $k_{\lambda t}$ is a mass attenuation coefficient with units of area per unit mass and ρ is the density of the medium. $k_{\lambda t}$ represents the effective area intercepting the radiation field per unit mass of substance contained within the volume.

Energy may be added to the beam through a scattering process by deflecting energy traveling in the direction of any other beam I'_λ into the direction of I_λ. Referring to the concept of the scattering phase function, $P(\bar{\theta})$, where $P(\bar{\theta})$ gives the probability that an incident intensity will be deflected through the required scattering angle $\bar{\theta}$ and be added to I_λ, the scattering contribution can be expressed as

$$+k_{\lambda t}\rho dsdAd\omega\int_0^{4\pi}P(\bar{\theta})I_\lambda' d\omega$$

Finally, the intensity of beam I_λ may be increased due to emission of energy by matter within the volume into the direction of propagation of I_λ. This contribution can be expressed as

$$+E_\lambda\rho dsdAd\omega$$

where E_λ is the rate of emission of energy per unit time per unit mass.

The change in intensity, dI_λ, with respect to distance of travel ds as the original incident beam passes through the unit volume can be expressed as the sum of the positive and negative changes. That is,

$$\frac{dI_\lambda}{ds}dsdAd\omega = -k_{\lambda t}\rho I_\lambda dsdAd\omega + k_{\lambda t}\rho dsdAd\omega\int_0^{4\pi}P(\bar{\theta})I_\lambda' d\omega' + E_\lambda\rho dsdAd\omega \quad (1)$$

Equation (1) can then be rewritten,

$$\frac{1}{\rho k_{\lambda t}}\frac{dI_\lambda}{ds} = J_\lambda - I_\lambda \quad (2)$$

where J_λ, known as the source term, is the sum of the source of the scattered radiation and the source of emitted radiation. Equation (2) represents the primitive form of the radiative transfer equation.

In achieving a solution to the radiative transfer equation similar to that accomplished in SPD for upward traveling radiation in the visible portion of the electromagnetic spectrum, several new terms are useful.

Optical thickness, τ_λ, of the attenuating medium is used as the z, or vertical, coordinate. τ_λ is defined by $d\tau_\lambda = -k_{\lambda t}\rho dz$. It is also convenient to replace the θ coordinate with $\mu = \cos\theta$. The azimuthal coordinate is defined as ϕ. Then, after making the following assumptions,

1) Horizontal homogeneity of the atmosphere

2) Time rate of change of I_λ is small compared to space rate of change

Equation (2) can be rewritten

$$\frac{-\mu dI_\lambda(\theta,\phi)}{d\tau_\lambda} = J_\lambda(\theta,\phi) - I_\lambda(\theta,\phi) \qquad (3)$$

The radiative transfer equation can be solved by the following method. Multiplying (3) by $e^{-\tau/\mu}$ and regrouping, with the subscript λ understood,

$$\mu e^{-\tau/\mu} \frac{dI(\tau,\mu,\phi)}{d\tau} - I(\tau,\mu,\phi)e^{-\tau/\mu} = -J(\tau,\mu,\phi)e^{-\tau/\mu}$$

or, equivalently,

$$\mu \frac{d}{d\tau}\left[I(\tau,\mu,\phi)e^{-\tau/\mu}\right] = -e^{-\tau/\mu}J(\tau,\mu,\phi)$$

In this solution, radiation is assumed to be traveling upward from the terrestrial surface to the level of the sensor. Therefore, the optical depth at the sensor for upward traveling radiation is zero. Let τ_s represent the optical depth between the surface and the level of the sensor, and let τ' represent the optical depth between the sensor and any level between the surface and the sensor.

Then, summing up all changes in the intensity of the beam as it passes through all intermediate levels τ' between the surface and the sensor,

$$\int_{\tau'=\tau_s}^{\tau'=0} d\left[I(\tau',\mu,\phi)e^{-\tau'/\mu}\right] = \int_{\tau'=\tau_s}^{\tau'=0} e^{-\tau'/\mu} J(\tau',\mu,\phi) \frac{d\tau'}{\mu}$$

or,

$$I(0,\mu,\phi) - I(\tau_s,\mu,\phi)\, e^{-\tau_s/\mu} = -\int_{\tau'=\tau_s}^{\tau'=0} e^{-\tau'/\mu} J(\tau',\mu,\phi) \frac{d\tau'}{\mu}$$

and,

[A] [B] [C]

$$I(0,\mu,\phi) = I(\tau_s,\mu,\phi)\, e^{-\tau_s/\mu} + \int_{\tau'=0}^{\tau'=\tau_s} e^{-\tau'/\mu} J(\tau',\mu,\phi) \frac{d\tau'}{\mu} \qquad (4)$$

Equation (4) represents a formal solution to the radiative transfer equation for upward traveling intensities in a horizontally homogeneous atmosphere. Term A gives the measured intensity at the sensor coming from

a direction defined by μ and ϕ. Term B represents the contribution to the measured intensity due to radiant energy leaving the surface. In SPD, the surface is assumed to have Lambertian reflecting characteristics. Hence, term B would consist of the incident solar radiation multiplied by the reflectivity of the surface and divided by π. Term C represents the source term, that is the contribution to measured intensity due to the presence of an atmospheric layer of optical depth τ_s.

Since the radiation considered here is in the visible portion of the spectrum, the source function term can be simplified. The wavelength at which an object emits radiation is a function of the temperature of the potential emitter. To emit appreciable amounts of radiation in the 0.4 to 0.7 μm range, a temperature of the order of several thousand degrees absolute is required. Since atmospheric constituents do not approach these temperatures, the emission term in the source function is dropped for radiative transfer studies of visible light. Hence, the source function consists only of the scattering term.

For the general case, the source function of term C of equation (4) can be written

$$J(\tau',\mu,\phi) = \underbrace{\frac{E(\tau',\mu,\phi)}{k_{\lambda t}}}_{[D]} + \underbrace{P(\mu,\phi,-\mu_o,\phi_o)\ F(\tau',-\mu_o,\phi_o)}_{[E]} + \int_o^{4\pi} P(\mu,\phi,\mu',\phi')\ I(\tau',\mu',\phi')d\omega' \qquad (5)$$

where the subscript o refers to incident solar radiation and $-\mu$ refers to a downward direction of travel. Term D of Equation (5) represents the contribution to intensity due to emission by atmospheric constituents at level τ'. For visible light, term D can be neglected. Term E represents the contribution to intensity due to the scattering of incident solar

flux at level τ' into the direction of travel defined by μ,ϕ. Term F represents the contribution to intensity propagating in the direction μ,ϕ due to the scattering at level τ' of radiation traveling in any other direction μ',ϕ' through the required scattering angle. Then, by substituting terms E and F of Equation (5) into Equation (4), the formal solution of the radiative transfer equation can be written

$$I(o,\mu,\phi) = I(\tau_s,\mu,\phi)e^{-\tau_s/\mu} + \int_{\tau'=0}^{\tau'=\tau_s} e^{-\tau'/\mu} \left[P(\mu,\phi,-\mu_o,\phi_o)\ F(\tau',-\mu_o,\phi_o) + \int_o^{4\pi} P(\mu,\phi,\mu',\phi')\ I(\tau',\mu',\phi')d\omega'\right]\frac{d\tau'}{\mu} \qquad (6)$$

Equation (6) represents the basic problem which is solved in SPD. It is through the first term on the r.h.s. of Equation (6) that the atmosphere can act as a filter of the signal, while it is through the second term on the r.h.s. that it can act as a signal generator. It is only in the unique situation when optical thickness is zero that the atmosphere can have no effect on the signal.

It is useful, at this point, to consider the manner in which the presence of a real atmosphere will actually produce changes in the intensity of a beam of interacting radiation by causing variations in the two terms on the right hand side of Equation (6). This discussion will be related to physical conditions encountered in a remote sensing field experiment.

Consider first the effect of changing the look angle, α, on the first term, which represents the attenuation of the beam of radiation traveling from the surface to the sensor. As look angle increases from zero, μ, which is cos (θ), decreases from unity. The magnitude of the negative exponent becomes larger, hence attenuation is greater. Therefore, since

intensities reflected by a Lambertian surface are of equal magnitude in all directions, the contribution by this term to the intensity sensed at a look angle, α, of 40° will be less than the value for a look angle of 0°.

The effect of a change in μ on the second term on the right hand side of Equation (6) will be of the opposite sign. Here, the effect of decreasing μ, hence increasing α, is to cause the computation of the source function contribution to be carried out over a longer path. This means that more molecules and aerosol particles will be available to scatter radiation into the direction of observation. Therefore, by changing look angles from 0° to 40°, the source function contribution to measured intensity will be increased. The amount of this increase will be further modified since the magnitude of the scattering phase function, present as a weighting factor inside the integral, is also determined by α.

The net result of the sum of the two terms on the r.h.s. of Equation (6) will, therefore, determine the shape of a graph showing intensities plotted against look angles. If variations in the first term dominate at all look angles across a flight line, the maximum point on the curve will occur at $\alpha = 0°$. If variations in the second term dominate at all look angles across the flight line, the maximum point will occur at the look angle which results in the largest combined contribution due to both path length and scattering phase function magnitude. Since both the first and second terms are non-linear, it is possible for domination to change as α increases from 0° to its maximum value. This will result in the occurrence of a secondary maximum or minimum. It is also possible for secondary extrema to occur as a result of rapid changes in the magnitude of the scattering phase function.

The location of any point on a curve can be physically interpreted by considering behavior of the surface term and of the source function. Intensity differences due solely to differing sensor altitudes or sensor orientations can also be analyzed using the same line of reasoning.

3.5.2 Optical Characteristics of the Atmosphere

Input to SPD includes the various atmospheric parameters required to determine the total scattering optical thickness and total absorption optical thickness of the atmospheric layers. The optical thicknesses are required to effect a solution of the radiative transfer equation.

Values used in this study for these atmospheric parameters were taken from a variety of sources. The atmosphere was assigned a barometric pressure value and an ozone concentration value at levels from the surface to 70 kilometers in accordance with Air Force Cambridge Research Laboratories Tables (McClatchey, et al., 1972) for midlatitude, summer conditions. Height-aerosol number density values between the surface and 70 kilometers were taken from sample computations performed by Dave (1972).

The Rayleigh scattering optical depth and ozone absorption coefficient, which are both wavelength dependent parameters, were taken from the Handbook of Geophysics (1961). The Mie scattering optical thickness and aerosol absorption optical thickness are based upon the aerosol index of refraction value which was taken from Deirmendjian (1969), and the aerosol size distribution function introduced in SPB.

3.5.3 Computational Parameters

Further input values to SPD specify the physical conditions for which the computation of intensities is desired. A solar zenith angle is designated for each run of SPD. In this study, zenith values analyzed were 0°,

20^{o}, and 40^{o}. Two intermediate atmospheric layer heights at which intensity computation results are desired are entered. This study selected 10,000 feet and 60,000 feet since these correspond to common remote sensing overflight altitudes. Computations are performed for twenty surface reflectivity values ranging from 0.0 to 1.0 during each run of SPD. This study covered the entire range using a reflectivity increment of .05, neglecting only .80. In the analysis of results, however, attention is primarily centered on surface reflectivities of .10 and .15, corresponding to reflectivity values for natural vegetation type surfaces. Finally, the number of azimuth angles, which define the angular separation of the plane of propagation and the plane of observation, is specified. Look angles used in computing results range from 0^{o} to 88^{o} at 2^{o} increments. Analysis of results is limited to look angles of 0^{o} to 40^{o} , since a deflection of 40^{o} is a reasonable limit for an airborne scanning system. Finally, the number of azimuth angles, which define the angular separation of the plane of propagation and the plane of observation, is specified. Results are computed for all azimuth angles from 0^{o} to 180^{o} at 10^{o} increments, with analysis of results performed when the azimuth angle equals 0^{o}, 90^{o}, and 180^{o}.

4. NUMERICAL RESULTS

4.1 Introduction

Numerical calculations performed in this study are based upon the assumption that the atmosphere is illuminated by π units of flux normal to the direction of propagation of the monochromatic, unidirectional solar radiation. The vertical downward flux at the top of the atmosphere is, therefore, equal to π multiplied by cos (θ_o) where θ_o is the zenith angle of the sun. Intensities calculated at a given level within the atmosphere are in relative units scaled to this input value. Results presented in this chapter show numerical changes in predicted intensity values as atmospheric, observation, and illumination parameters are varied.

If intensity of visible light is the measured parameter, remote sensing classifications of surface features are accomplished through estimation of surface reflectivities. Hence it is desirable to relate changes in the intensity of a signal caused by the presence of the atmosphere to changes in surface reflectivity which would result in an equivalent signal modification in the absence of an atmospheric effect.

4.2 Intensities in an Atmosphere with Zero Optical Thickness

If the atmosphere had zero optical thickness, the vertical downward flux at the surface would equal the vertical downward flux at the top of the atmosphere, that is $\pi \cdot \cos(\theta_o)$. Since the surface in the model is assumed to be Lambertian, the fraction of incident radiation specified by the reflectivity, r, will be reflected upward as an isotropic radiation field. In an isotropic field, the intensity in any direction equals the flux divided by π. Therefore, the magnitude of the upward intensity vector at any level for any sensor viewing angle would equal $r \cdot \pi \cdot \cos(\theta_o)/\pi$, or $r \cdot \cos(\theta_o)$.

At this point, it is useful to consider a numerical example. In this example, and in future numerical discussions, the term intensity will refer to the magnitude of the intensity vector. If $\theta_o = 0°$, $\cos(\theta_o) = 1.0$ and intensity = reflectivity. Thus a surface reflectivity of 0.10 would result in an upward intensity at any level of 0.1000 if the atmosphere had no modifying effect. Now consider an atmosphere with a non-zero optical thickness in a situation with exactly the same geometry. If the resultant computed intensity equaled 0.1100, this would be equivalent to an increase to 0.11 in surface reflectivity for zero optical thickness. That is, ΔI of 0.01 corresponds to Δr of 0.01 if $\theta_o = 0°$.

If $\theta_o = 20°$, $\cos(\theta_o) = 0.9400$, and a surface reflectivity of 0.10 would result in an intensity of 0.0940 in a zero optical thickness situation. For the same illumination and observation conditions, if inclusion of an interacting atmosphere resulted in a computed intensity of 0.1034 (note: $0.94 \cdot 0.11 = 0.1034$) this would be equivalent to increasing surface reflectivity to 0.11 if the atmosphere had remained at zero optical thickness; that is, Δr of 0.01 corresponds to ΔI of 0.0094 if $\theta_o = 20°$.

In this chapter, computed intensities resulting from the inclusion of a realistic atmosphere will be compared with expected intensities for the same geometry and surface reflectivity, but with a zero optical thickness atmosphere. Changes from the expected value will be discussed in terms of the equivalent change in surface reflectivity required to achieve the same solution for a zero optical thickness situation.

4.3 Directional Parameters and Scattering Angles

As stated in Chapter 2, molecular scattering is directionally dependent with forward scattering and backward scattering twice as great as side scattering. In comparison to molecular scattering, scattering by larger particles is highly anisotropic with a very large forward component and a secondary maximum in the backscattering direction. Due to the directional nature of the scattering process, intensity calculations are highly sensitive to the changes in scattering angle when computations are made across an aircraft flight line.

The scattering angle, $\bar{\theta}$, is defined as the angle between the directions of propagation and observation, which are defined in this study in terms of their angular displacement from local vertical and referred to as θ_o and θ, respectively. When the direction of propagation, the direction of observation, and vertical are coplanar the scattering process is said to occur in the principle plane. This geometry results in the maximum possible variation in scattering angles across an aircraft flight line. In this situation θ_o and θ are contained within the same plane and have a common side, the local vertical. Therefore any change in θ, or equivalently in the look angle α, for a fixed θ_o during a sweep across the flight line will result in the same change in scattering angle. If scattering is not computed in the principle plane, the one-to-one correspondence between $\Delta\bar{\theta}$ and $\Delta\alpha$ will not occur and $\Delta\bar{\theta}$ will be smaller than $\Delta\alpha$.

In this study, the look angles, α, to the right of zero on the abscissa of intensity graphs refer to the situation in which the azimuth displacement, with reference to the sensor, between the plane containing θ_o and the plane containing α is between 0° and 90°; the left side of

zero corresponds to azimuthal displacement of 90° to 180°. The importance of the orientation of the sensing plane in relation to the direction of propagation will be illustrated in a quantitative sense later in this chapter.

4.4 Modification of Intensities in a Pure Rayleigh Atmosphere

Before considering an atmosphere containing an aerosol, it is useful to consider the modification of intensities caused solely by the molecular components of the atmosphere. Consequently, SPD was run for both wavelengths considered in this study, 0.45 μm and 0.70 μm, for an atmosphere containing no aerosol particles. Figure 4-1 shows the results of these computations with the dashed lines showing intensities when the incident radiation is at 0.45 μm, while the solid lines show the results when illumination is at 0.70 μm. Intensities are plotted for an altitude of approximately 10,000 feet at look angles ranging from 40° left of nadir to 40° right of nadir. The surface reflectivity selected was 0.10, a representative value for natural vegetation reflectivity at these wavelengths. Hence, intensities for an atmosphere with zero optical thickness would be 0.1000 for $\theta_o = 0°$, 0.0940 for $\theta_o = 20°$, and 0.0766 for $\theta_o = 40°$. These results are computed for principle plane scattering.

It is immediately apparent from Figure 4-1 that the atmospheric effect for molecular scattering is greater when illumination is at 0.45 μm than when illumination is at 0.70 μm. This is consistent with Lord Rayleigh's approximation which states that scattering is inversely proportional to the fourth power of wavelength.

Due to the much larger source function contribution at the shorter wavelength, the $\theta_o = 0°$ curve for $\lambda = 0.45$ μm shows an atmospheric intensity modification equivalent to a zero optical thickness surface reflectivity change of about 0.014. At $\lambda = 0.70$ μm, the source function contribution is smaller and is almost balanced out by attenuation of the surface term. The equivalent surface reflectivity change at the longer wavelength is about 0.0015.

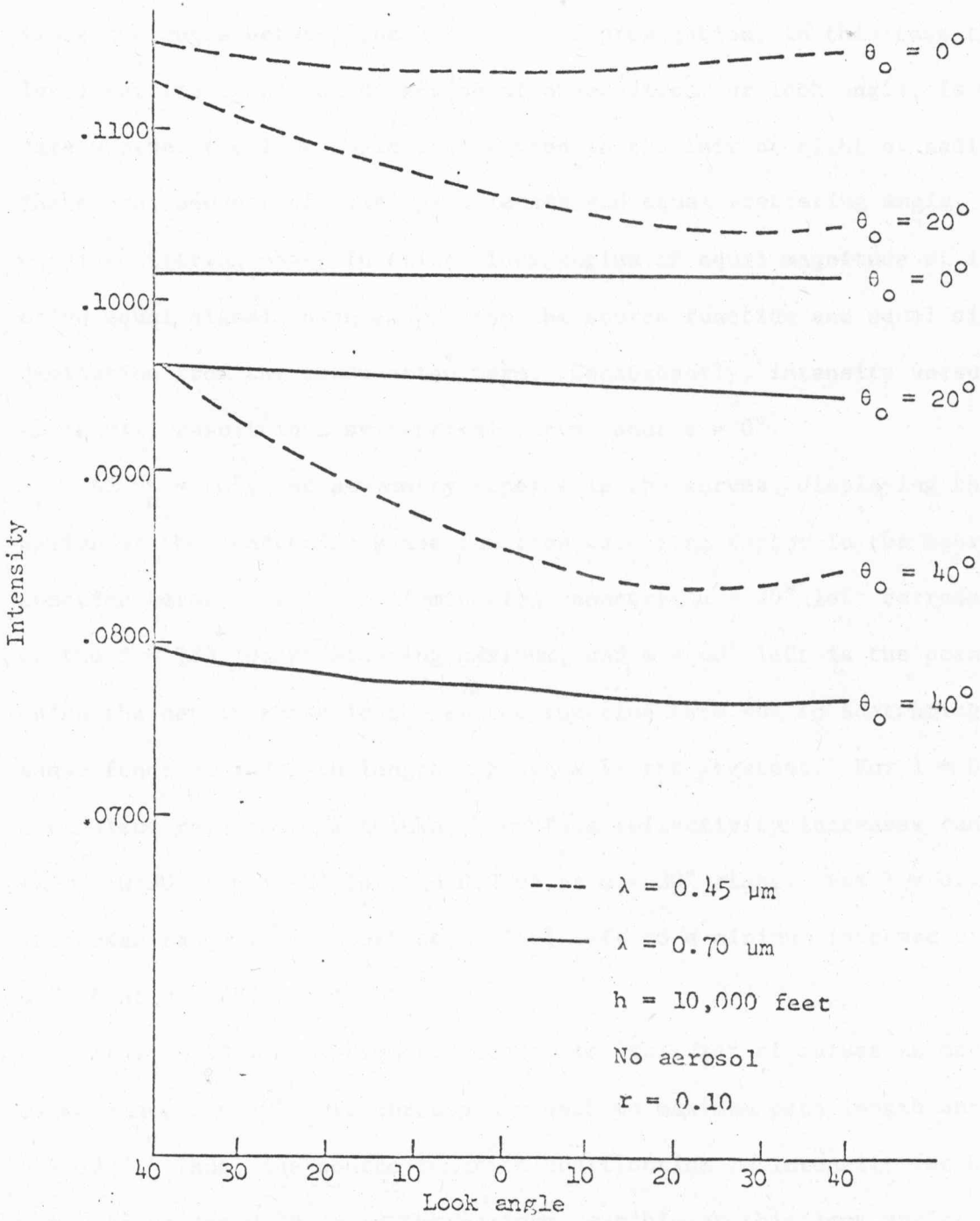

Figure 4-1 Intensitv Modifications in a Rayleigh Atmosphere

Graphs of intensity versus look angle will always be symmetrical about the point $\alpha = 0°$. Look angles of equal magnitude result in path lengths from the sensor to the surface of equal distance. Also, look angles of equal magnitude result in scattering angles of equal magnitude since the angle between the direction of propagation, in this case the local vertical, and the direction of observation, or look angle, is the same whether the look angle is measured to the left or right of nadir. Therefore, because of equal path length and equal scattering angle, hence equal scattering phase function, look angles of equal magnitude will receive equal signal enhancement from the source function and equal signal diminution from the attenuation term. Consequently, intensity versus look angle will result in a symmetrical curve about $\alpha = 0°$.

At $\theta_o = 20°$, the asymmetry appears in the curves, displaying the behavior of the scattering phase function weighting factor in the source function term. For this illumination geometry, $\alpha = 20°$ left corresponds to the $\bar{\theta} = 180°$ backscattering maximum, and $\alpha = 40°$ left is the point at which the net increase in the source function term due to scattering phase function and path length magnitude is the greatest. For $\lambda = 0.45$ μm, equivalent zero optical thickness surface reflectivity increases range from 0.0200 at $\alpha = 40°$ left to 0.0106 at $\alpha = 30°$ right. For $\lambda = 0.70$ μm, increases range from 0.0025 at $\alpha = 40°$ left to a minimum increase of 0.0006 at $\alpha = 38°$ right.

At $\theta_o = 40°$, the asymmetry factor for this set of curves is maximized since $\alpha = 40°$ left corresponds both to maximum path length and to $\bar{\theta} = 180°$. Thus, the source function contribution to intensity for both $\lambda = 0.45$ μm and 0.70 μm is the maximum possible at this look angle. At

the shorter wavelength, equivalent surface reflectivity increases range from 0.0261 to 0.0086. At the longer wavelength, increases range from 0.0035 to 0.0001.

4.5 Intensity Modification by an Atmosphere Containing Aerosols

As previously stated, large particles scattering is highly anisotropic. The scattering phase function magnitude can change very rapidly as look angle changes. This causes the source function contribution to intensity to be more sensitive to look angle if an aerosol is present than if the atmosphere is characterized by only Rayleigh scattering. Consequently, graphs of intensity versus look angle may show rapid fluctuations which can be interpreted only through consideration of scattering phase function values.

Figure 4-2 shows the scattering phase function plotted versus scattering angle for the three aerosol - incident radiation combinations considered in this study. The solid line represents an atmosphere containing a silicate aerosol, with index of refraction m = 1.56 - 0.00i, under illumination by radiation at 0.70 μm. The dashed line displays the scattering properties of a water droplet aerosol, with m = 1.33 - 0.00i, when incident radiation is at 0.70 μm. The dotted line corresponds to the water droplet aerosol, m = 1.33 - 0.00i, when λ = 0.45 μm. The imaginary term in the index of refraction reflects the absorption potential of the aerosol while the real term is a measure of the scattering properties. Hence, all aerosol populations considered here are non-absorbent.

Scattering phase function values are shown in Figure 4-2 for scattering angles from 100° to 180° because the geometrical limits of this study, maximum θ_o = 40° and maximum α = 40°, restrict possible scattering angles encountered to this range. The values for the scattering phase function for all possible scattering angles are determined by computer solution of the Mie equations, however, and received in this series of programs as

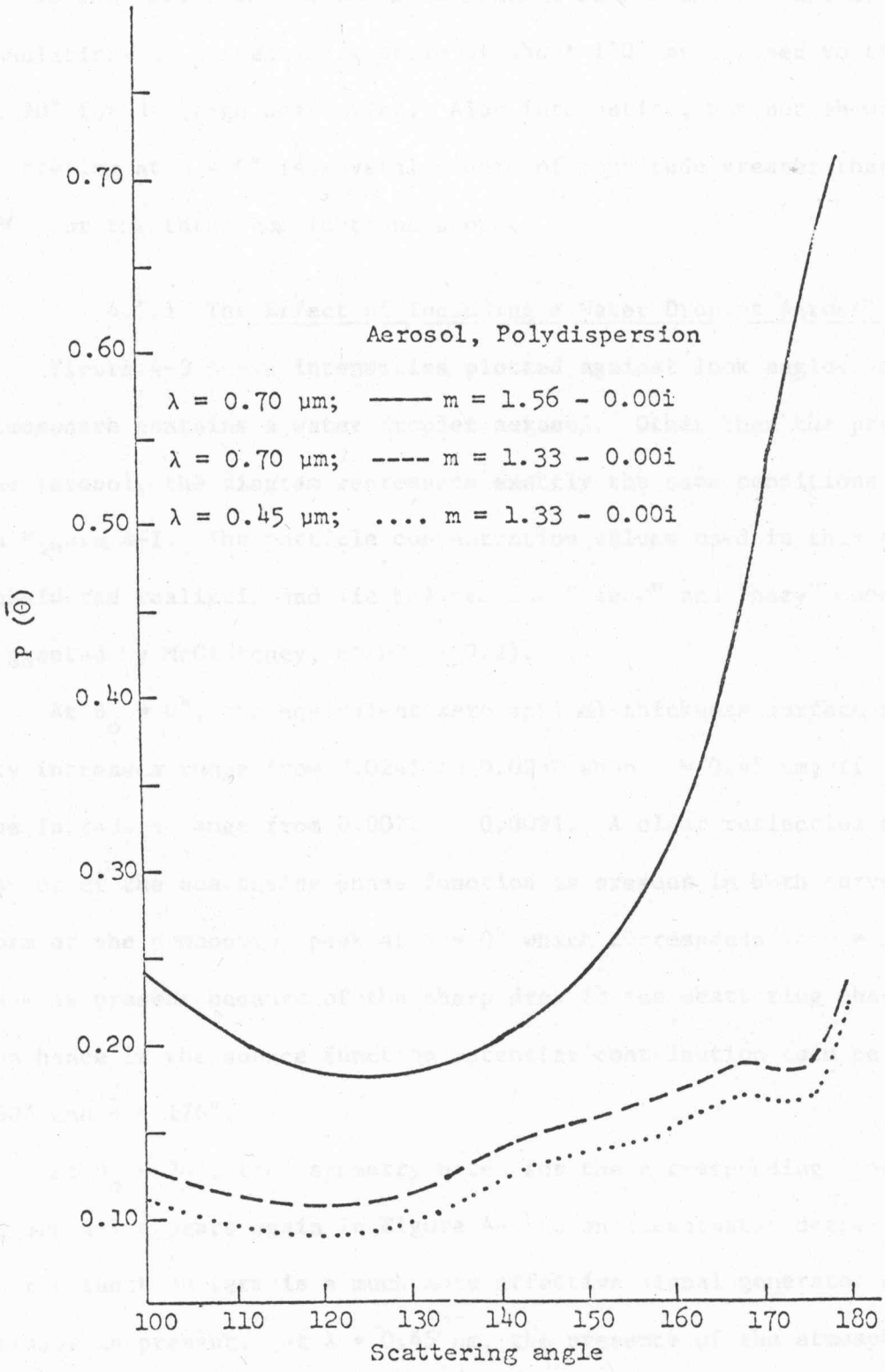

Figure 4-2 Scattering Phase Function Values

output from both SPB and SPC. An important feature to notice in Figure 4-2 is that all three curves show minimum scattering for the aerosol populations at a scattering angle of about 120° as opposed to the minimum at 90° for Rayleigh scattering. Also interesting, but not shown, is that scattering at $\bar{\theta} = 0°$ is several orders of magnitude greater than at $\bar{\theta} = 180°$ for the three combinations shown.

4.5.1 The Effect of Including a Water Droplet Aerosol

Figure 4-3 shows intensities plotted against look angles when the atmosphere contains a water droplet aerosol. Other than the presence of the aerosol, the diagram represents exactly the same conditions depicted in Figure 4-1. The particle concentration values used in this study are considered realistic and lie between the "clear" and "hazy" concentrations suggested by McClatchey, et al. (1972).

At $\theta_o = 0°$, the equivalent zero optical thickness surface reflectivity increases range from 0.0241 to 0.0250 when $\lambda = 0.45$ μm; if $\lambda = 0.70$ μm, the increases range from 0.0072 to 0.0091. A clear reflection of the behavior of the scattering phase function is present in both curves in the form of the pronounced peak at $\alpha = 0°$ which corresponds to $\theta = 180°$. This peak is present because of the sharp drop in the scattering phase function, and hence in the source function intensity contribution term between $\bar{\theta} = 180°$ and $\bar{\theta} = 176°$.

At $\theta_o = 20°$, the asymmetry noted for the corresponding lines in Figure 4-1 appears again in Figure 4-3 to an accentuated degree since the source function term is a much more effective signal generator when an aerosol is present. At $\lambda = 0.45$ μm, the presence of the atmosphere causes intensity increases ranging from 0.0319 at $\alpha = 40°$ left to the minimum

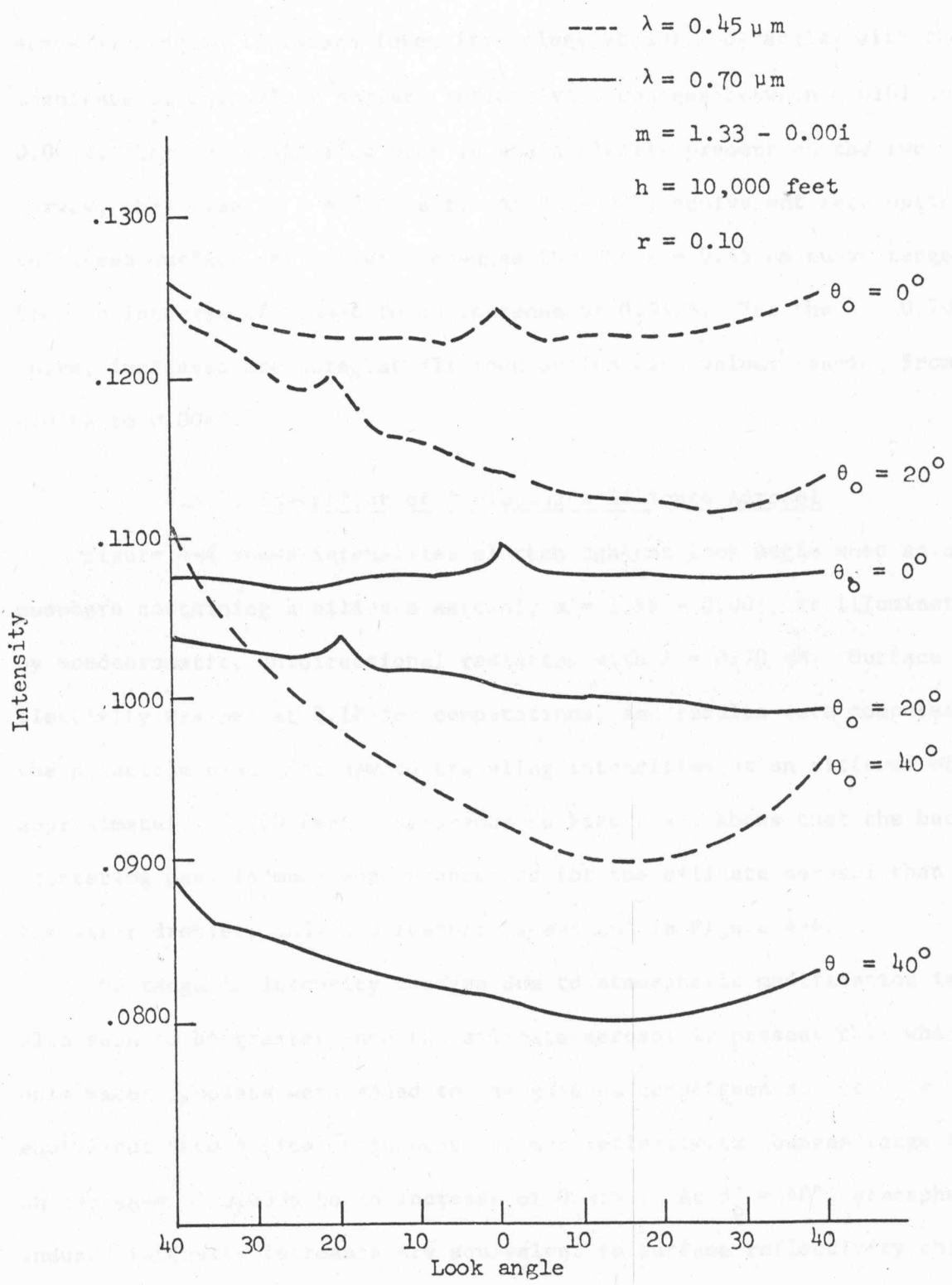

Figure 4-3 Intensity Modifications by an Atmosphere Containing a Water Droplet Aerosol

increase of 0.0185 at $\alpha = 26°$ right. For $\lambda = 0.70$ μm, the presence of the atmosphere again increases intensity values at all look angles with the magnitude of equivalent surface reflectivity changes between 0.0101 and 0.0052. The backscattering peak is again clearly present on the two curves, this time at $\alpha = 20°$ left. At $\theta_o = 40°$, equivalent zero optical thickness surface reflectivity changes for the $\lambda = 0.45$ μm curve range from an increase of 0.0446 to an increase of 0.0173. For the $\lambda = 0.70$ μm curve, increases are noted at all look angles with values ranging from 0.0162 to 0.0049.

4.5.2 The Effect of Including a Silicate Aerosol

Figure 4-4 shows intensities plotted against look angle when an atmosphere containing a silicate aerosol, $m = 1.56 - 0.00i$, is illuminated by monochromatic, unidirectional radiation with $\lambda = 0.70$ μm. Surface reflectivity was set at 0.10 for computations, and results were computed in the principle plane for upward traveling intensities at an altitude of approximately 10,000 feet. Reference to Figure 4-2 shows that the backscattering peak is much more pronounced for the silicate aerosol than for the water droplet, and this feature is evident in Figure 4-4.

The range in intensity changes due to atmospheric modification is also seen to be greater when the silicate aerosol is present than when only water droplets were added to the gaseous constituents. At $\theta_o = 0°$, equivalent zero optical thickness surface reflectivity changes range from an increase of 0.0356 to an increase of 0.0159. At $\theta_o = 40°$, atmosphere induced intensity increases are equivalent to surface reflectivity changes of 0.0602 to 0.0140.

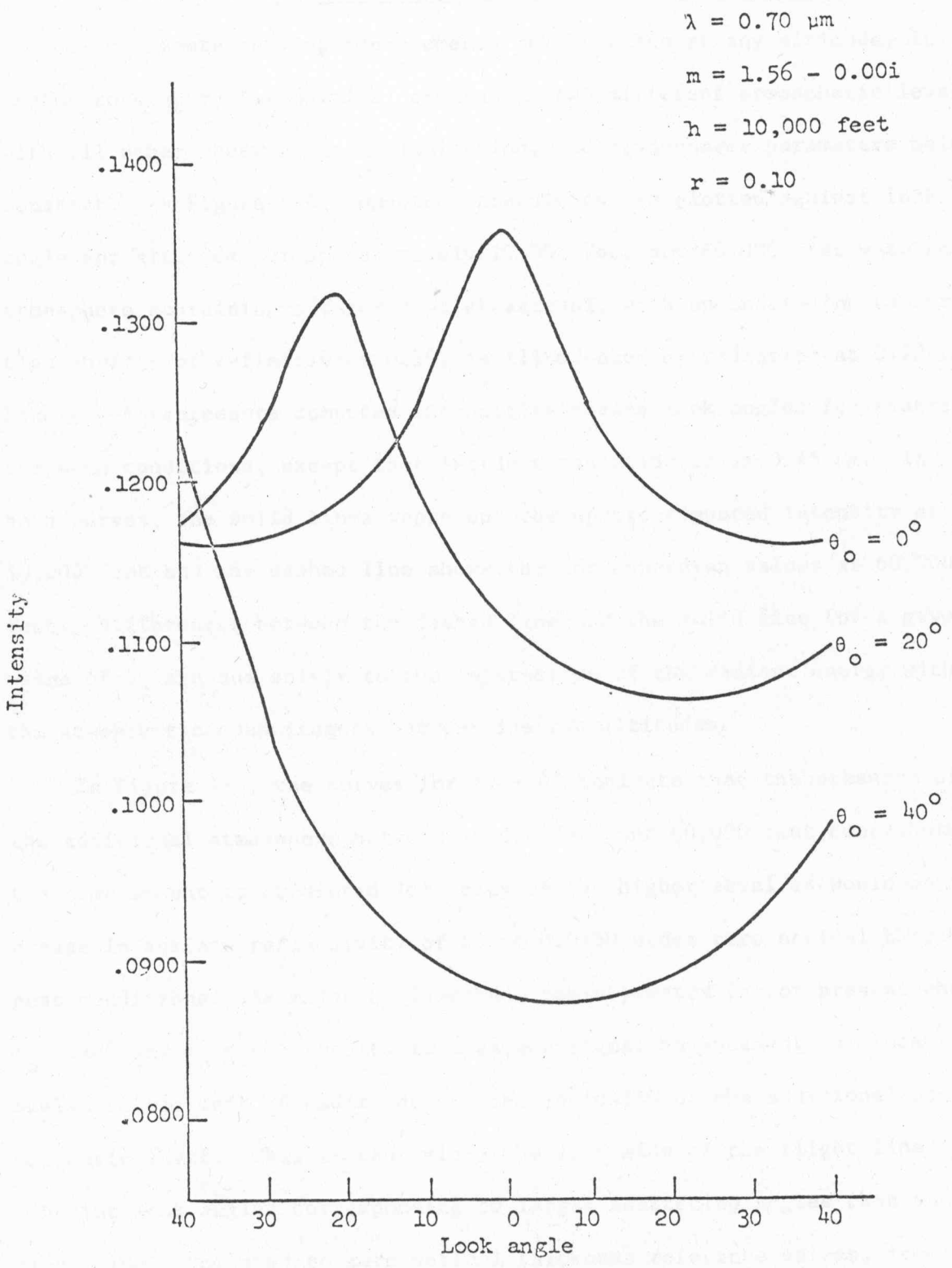

Figure 4-4 Intensity Modifications by an Atmosphere Containing a Silicate Aerosol

4.5.3 The Effects of Observation Altitude on Intensities

Since remote sensing measurements may be taken at any altitude, it is useful to compare intensities computed at two different atmospheric levels, with all other observation, illumination, and atmospheric parameters held constant. In Figure 4-5, computed intensities are plotted against look angle for altitudes of approximately 10,000 feet and 60,000 feet when an atmosphere containing a water droplet aerosol, with an underlying Lambertian surface of reflectivity 0.10, is illuminated by radiation at 0.70 μm. Figure 4-6 represents computed intensities versus look angles for exactly the same conditions, except that incident radiation is at 0.45 μm. In both curves, the solid lines represent the upward computed intensity at 10,000 feet and the dashed line shows the corresponding values at 60,000 feet. Differences between the dashed line and the solid line for a given value of θ_o are due solely to the interaction of the radiant energy with the atmospheric constituents between the two altitudes.

In Figure 4-5, the curves for $\theta_o = 0°$ indicate that the presence of the additional atmosphere between 10,000 feet and 60,000 feet contributes the same amount to predicted intensity at the higher level as would an increase in surface reflectivity of about 0.0150 under zero optical thickness conditions. As might be expected, the asymmetry factor present when $\theta_o = 20°$ and $\theta_o = 40°$ results in a larger signal enhancement for look angles to the left of nadir due to the inclusion of the additional atmospheric layer. This is true since the left side of the flight line contains look angles corresponding to larger scattering angles than the right side. Compared to zero optical thickness reference values, increases in surface reflectivity due to the additional atmospheric layer reach 0.0101 for $\theta_o = 20°$ and 0.0137 for $\theta_o = 40°$. Thus, for example,

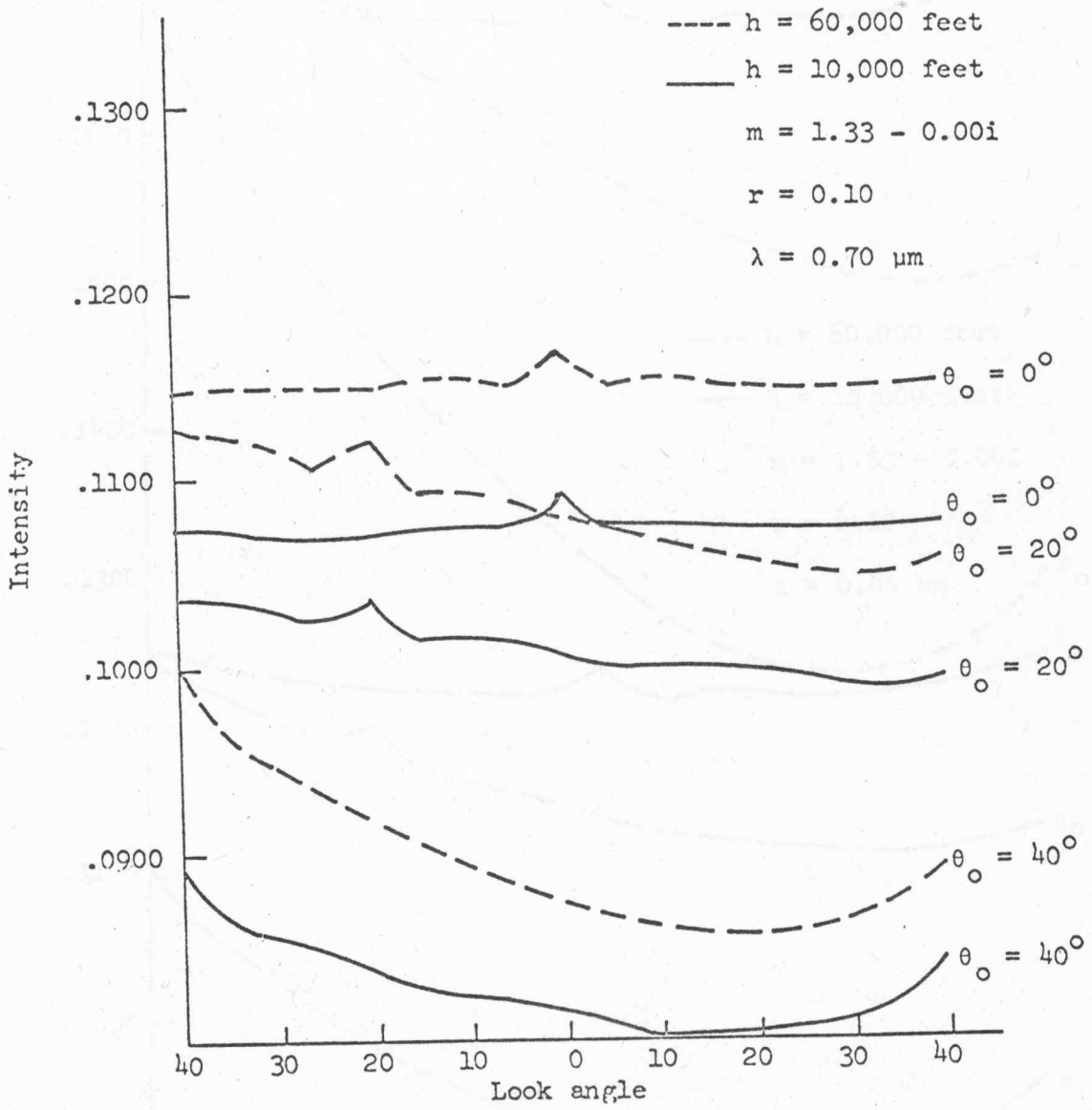

Figure 4-5 The Effects of Measurement Altitude on Intensities; $\lambda = 0.70$ μm

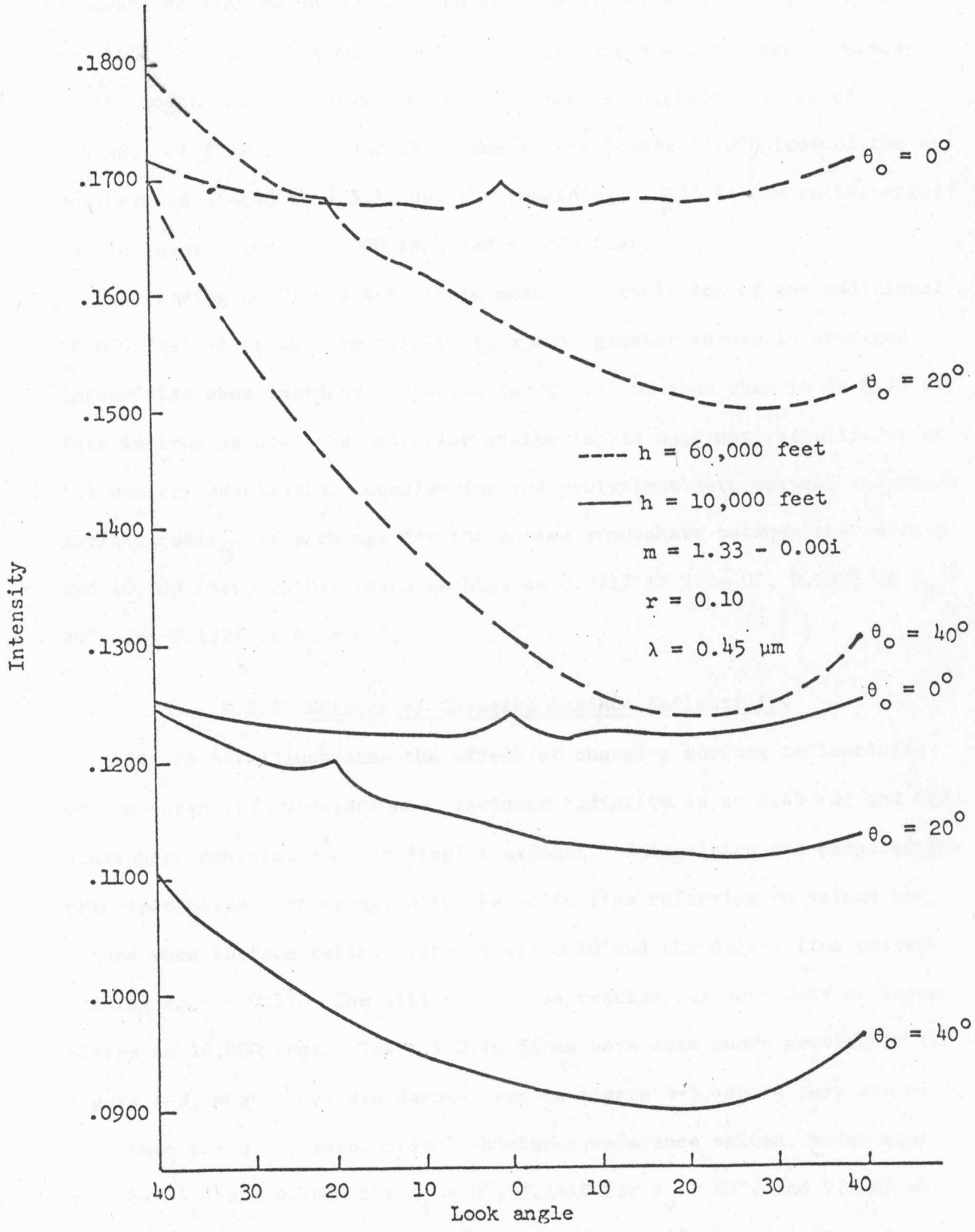

Figure 4-6 The Effects of Measurement Altitude on Intensities; $\lambda = 0.45$ μm

a remote sensing measurement taken at 60,000 feet with $\theta_o = 40°$ and $\alpha = 40°$ left corresponding to a 180° scattering angle would sense an atmospheric contribution equivalent to a surface reflectivity change of 0.0299. Of this total, 0.0162 is due to the lowest 10,000 feet of the atmosphere as stated in 4.5.1, and the remaining 0.0137 is due to the atmospheric layer between 10,000 feet and 60,000 feet.

Referring to Figure 4-6, it is seen that inclusion of the additional 50,000 feet of atmosphere results in a much greater change in prediced intensities when incident radiation is at 0.45 μm than when it is 0.70 μm. This is true because the molecular scattering is much more significant at the shorter wavelength. Considering the equivalent zero optical thickness surface reflectivity change for the entire atmosphere between the surface and 60,000 feet, values reach as high as 0.0717 if $\theta_o = 0°$, 0.0906 if $\theta_o = 20°$, and 0.1223 if $\theta_o = 40°$.

4.5.4 Effects of Changing Surface Reflectivity

Figure 4-7 illustrates the effect of changing surface reflectivity on the intensity calculations. Incident radiation is at 0.45 μm, and the atmosphere contains a water droplet aerosol. Intensities are computed for principle plane scattering, with the solid line referring to values obtained when surface reflectivity equals 0.10 and the dashed line corresponding to r = 0.15. The altitude of observation for both sets of intensities is 10,000 feet. The r = 0.10 lines have been shown previously in Figure 4-3, where they are dashed, and in Figure 4-5, where they are solid.

When r = 0.15, zero optical thickness reference values, which equal r x cos (θ_o) are 0.1500 for $\theta_o = 0°$, 0.1410 for $\theta_o = 20°$, and 0.1149 when $\theta_o = 40°$. With the higher reflectivity and $\theta_o = 0°$, equivalent zero

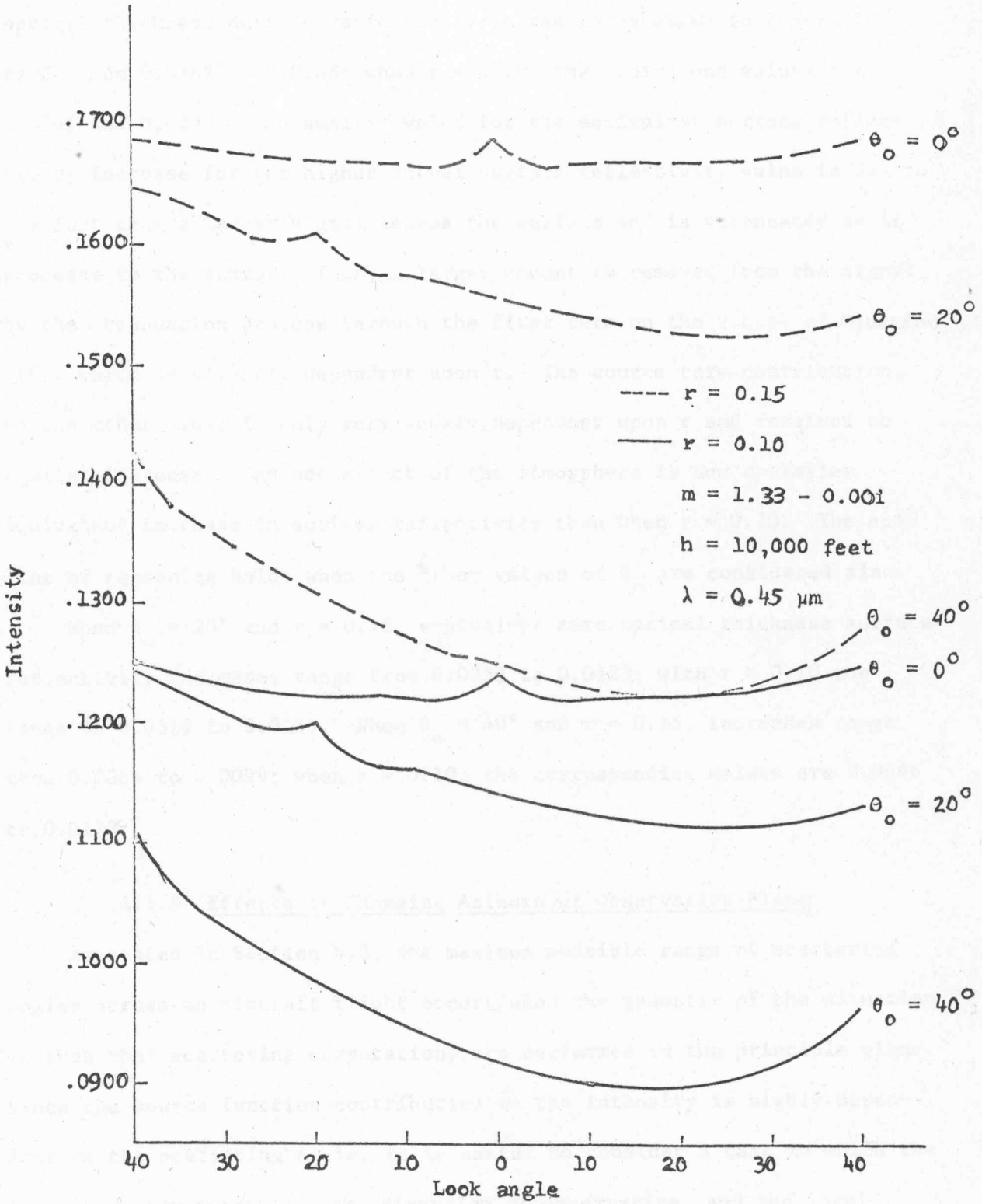

Figure 4-7 The Effects of Changing Surface Reflectivities on Intensities; m = 1.33 - 0.00i

optical thickness surface reflectivity increases as shown in Figure 4-7 range from 0.0167 to 0.0188; when r = 0.10, the equivalent values are 0.0241 and 0.0250. The smaller value for the equivalent surface reflectivity increase for the higher actual surface reflectivity value is due to the fact that a larger signal leaves the surface and is attenuated as it proceeds to the sensor. Thus, a larger amount is removed from the signal by the attenuation process through the first term on the r.h.s. of Equation (6) which is directly dependent upon r. The source term contribution, on the other hand, is only very weakly dependent upon r and receives no similar increase. The net effect of the atmosphere is now a smaller equivalent increase in surface reflectivity than when r = 0.10. The same line of reasoning holds when the other values of θ_o are considered also.

When $\theta_o = 20°$ and r = 0.15, equivalent zero optical thickness surface reflectivity increases range from 0.0252 to 0.0123; with r = 0.10 the range is 0.0319 to 0.0185. When $\theta_o = 40°$ and r = 0.15, increases range from 0.0364 to 0.0099; when r = 0.10, the corresponding values are 0.0446 to 0.0173.

4.5.5 Effects of Changing Azimuth of Observation Plane

As stated in Section 4.3, the maximum possible range of scattering angles across an aircraft flight occurs when the geometry of the situation is such that scattering computations are performed in the principle plane. Since the source function contribution to the intensity is highly dependent on the scattering angle, it is useful to consider a case in which the direction of propagation, the direction of observation, and the local vertical are not coplanar and hence, the range of scattering angles covered is diminished.

Figure 4-8 shows results of computations performed when the plane containing the local vertical and the direction of propagation is rotated 90^{o} from the plane containing the local vertical and the direction of observation. In Figure 3-1, this corresponds to the solar zenith angle being contained in the yz plane and the look angle being contained in the xz plane.

The change in geometry affects intensity computations only when θ_o is other than 0°, since positioning the illuminating source such that the direction of propagation is the local vertical ensures that the solar zenith angle and the look angle will be coplanar. Therefore, Figure 4-8, which depicts exactly the same conditions as Figure 4-7 except that the plane containing the various values of α has been rotated 90°, contains $\theta_o = 0°$ values only for reference purposes.

When $\theta_o = 20°$, scattering angles decrease in a non-linear fashion from 160° at $\alpha = 0°$ to 136.04° at $\alpha = 40°$ left and right. The range of equivalent surface reflectivity increases shown in Figure 4-8 when $\theta_o = 20°$ and $r = 0.10$ is 0.0249 to 0.0212 compared to the range 0.0319 to 0.0185 for principle plane geometry shown in Figure 4-6. When $\theta_o = 20°$ and $r = 0.15$, zero optical thickness equivalent surface reflectivity increases shown in Figure 4-8 range from 0.0183 to 0.0153 compared to principle plane results ranging from 0.0252 to 0.0123. Thus, the net effect of rotating the plane of observation 90° is to reduce the maximum and increase the minimum in equivalent surface reflectivity changes. This is true because the scattering phase function weighting factor in the source function contribution no longer includes values corresponding to scattering angles between 160° and 180°, the largest values on the scattering phase function curve (Figure 4-2), and it no longer includes values

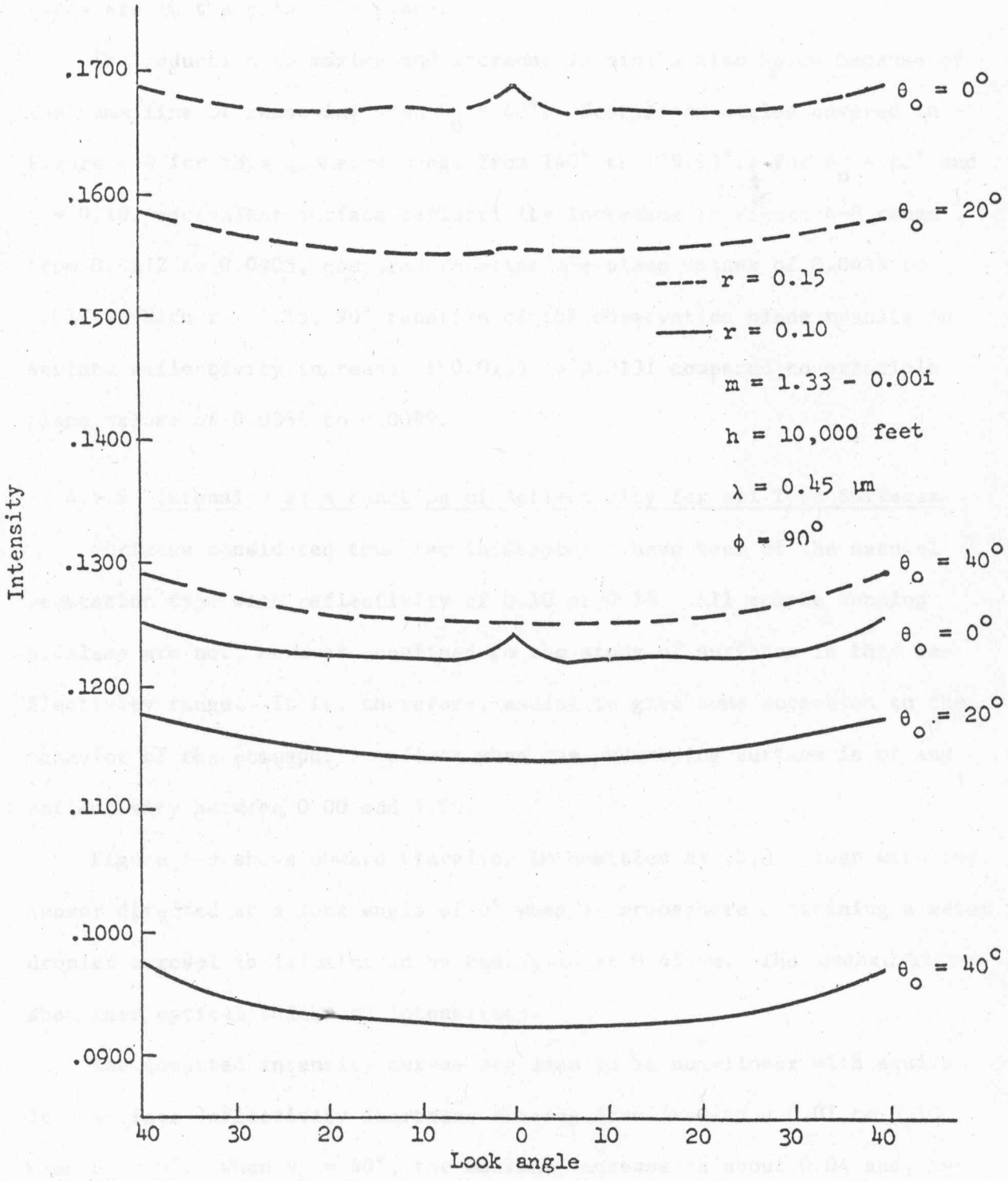

Figure 4-8 The Effects of Rotating Observation Plane on Intensities

between $\bar{\theta}$ = 136.04° and 120°, the minimum range when θ_o = 20° and computations are in the principle plane.

The reduction in maxima and increase in minima also holds because of the same line of reasoning when θ_o = 40°. Scattering angles covered in Figure 4-8 for this geometry range from 140° to 125.93°. For θ_o = 40° and r = 0.10, equivalent surface reflectivity increases in Figure 4-8 range from 0.0272 to 0.0205, compared to principle plane values of 0.0446 to 0.0173. With r = 0.15, 90° rotation of the observation plane results in surface reflectivity increase of 0.0155 to 0.0131 compared to principle plane values of 0.0364 to 0.0099.

4.5.6 Intensity as a Function of Reflectivity for all Type Surfaces

Surfaces considered thus far in Chapter 5 have been of the natural vegetation type with reflectivity of 0.10 or 0.15. All remote sensing problems are not, however, confined to the study of surfaces in this reflectivity range. It is, therefore, useful to give some attention to the behavior of the atmospheric effect when the underlying surface is of any reflectivity between 0.00 and 1.00.

Figure 4-9 shows upward traveling intensities at 10,000 feet with the sensor directed at a look angle of 0° when an atmosphere containing a water droplet aerosol is illuminated by radiation at 0.45 μm. The dashed lines show zero optical thickness intensities.

The computed intensity curves are seen to be non-linear with equivalent surface reflectivity increases ranging from less than 0.01 to 0.10 when θ_o = 0°. When θ_o = 40°, the maximum increase is about 0.04 and, between reflectivities of 0.25 and 0.75 the atmosphere has the net effect of a signal filter, with an equivalent surface reflectivity decrease of as

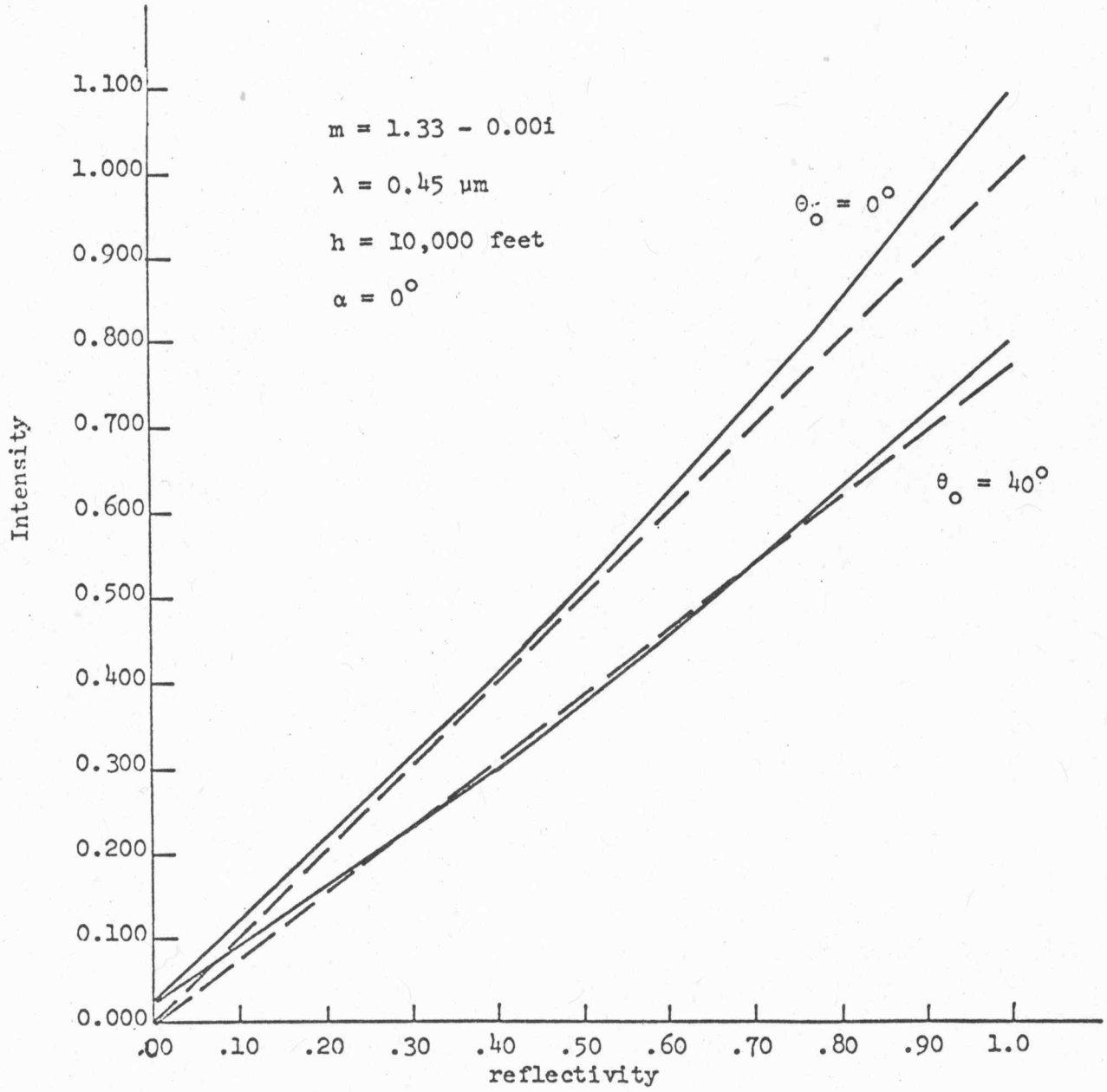

Figure 4-9 Intensities at All Surface Reflectivities

much as 0.01. A discussion of the implications of this diagram will be given at the end of the next chapter.

5. DISCUSSION OF RESULTS AND CONCLUSIONS

Results of computations presented in Chapter 4 demonstrate, on a quantitative basis, the presence of a modifying effect on radiant intensities due to the existence of an interacting atmosphere. The magnitude of the effect varies noticeably when parameters such as the wavelength of incident radiation, solar zenith angle, observation altitude and direction, type of aerosol present, underlying surface reflectivity, and orientation of sensing plane are changed.

It is impossible to state that an atmospheric effect of any particular magnitude will cause an incorrect classification of a surface feature to be made. If an investigator were forearmed with a general knowledge of the target area, and merely wished to discriminate between features of grossly different reflectivity characteristics, it is very possible that the atmosphere would be incapable of masking these differences. However, as required discriminations become more refined and the need for absolute accuracy in surface reflectivity data increases, the importance of considering the presence of the atmosphere will also increase. It is under circumstances in which a high degree of accuracy in estimates of surface reflectivities is required that the results in Chapter 4 would be most important. These results not only provide an

investigator with an idea of the magnitude of the atmospheric effect and hence its importance in relation to his particular problem, they also suggest ways in which this atmospheric effect may be minimized.

Absolute values for the equivalent changes in surface reflectivity for a given situation can be taken directly from the figures presented in Chapter 4. In this concluding section of the study, attention will be directed at the behavior of the curves presented in the previous section. Through analysis of the variations noted in the range of equivalent surface reflectivity changes across a particular aircraft flight line, it is possible to suggest ways in which the range of equivalent surface reflectivity changes caused by the presence of the atmosphere may be minimized. The behavior patterns which appear are the result of interaction between the source function term and the attenuation term in the radiative transfer equation.

The source function term, weighted by the scattering phase function, strengthens the signal measured at the sensor. The attenuation term reduces the magnitude of the measured intensity. The equivalent surface reflectivity change is simply a measure of the difference in their magnitudes. To minimize the atmospheric effect, the correct technique is to make them as nearly equal in absolute value as possible. In this manner, measured surface reflectivities will be as close as possible to the actual absolute value of surface reflectivity. Let us now consider the mechanisms by which variations in physical parameters affect the measured intensity.

The altitude at which intensity measurements are made is a parameter which can be changed with predictable results on the range of changes in

equivalent zero optical thickness surface reflectivity. By increasing measurement altitude, only path length is changed for a given look angle. If the path length is increased, the source function contribution will be increased, the amount of this increase being dependent on the magnitude of the scattering phase function. On the other hand, the attenuation term is also increased in magnitude. If the source function dominates, the atmosphere will act as a signal generator, and its net contribution will be greater at the higher altitude. This is illustrated in Figures 4-5 and 4-6 where intensities, and therefore equivalent surface reflectivity changes, are greater at the higher altitude for any given θ_o. The increase is more noticeable when the incident radiation is at 0.45 μm since the Rayleigh scattering is very strong at the shorter wavelengths and provides a significant increase to the source term.

A more complex interaction between the terms comprising the atmospheric effect is well illustrated through the analysis of equivalent surface reflectivity changes across an aircraft flight line resulting if only the solar zenith angle is changed. Figure 4-3 is a useful reference for this discussion, and it should be remembered that changes in intensity must be divided by cos (θ_o) to numerically evaluate equivalent changes in surface reflectivity.

First consider the case where $\theta_o = 0°$. As the look angle increases from zero, the path length increases and the scattering angle decreases. The increase in path length simultaneously affects the different terms in the atmospheric contribution to measured intensity: it is increased through a greater source function contribution and is decreased by greater attenuation. Further, the decrease in scattering angle decreases

the amount the atmosphere is able to contribute to the intensity due to the appearance of the scattering phase function as a weighting factor in the source term. The net effect of these actions and interactions is a relatively small increase in equivalent surface reflectivity.

Consider now the case where $\theta_o = 20°$. Here, a scattering angle of 180° occurs at a look angle of 20° left. Thus, the strongest possible scattering phase function weighting value is now combined with the path length corresponding to $\alpha = 20°$ rather than $\alpha = 0°$. The source function contribution is now much greater at $\alpha = 20°$ left than it was when $\theta_o = 0°$. The attenuation term is unchanged, however, since a look angle of 20° left corresponds to the same path length no matter what the solar zenith angle. At a look angle of 40° left, the scattering angle with $\theta_o = 20°$ is now 160° as opposed to 140° when $\theta_o = 0°$. Thus the source function is again increased by moving the solar zenith angle from 0° to 20° but the attenuation term is unchanged. The fact that less radiation enters the atmosphere to contribute to the source function at the greater solar zenith angle is compensated for by the fact that less radiation is reflected by the surface to be attenuated. The net result of these actions and interactions is that larger equivalent surface reflectivity changes are present at look angles on the left edge of the aircraft flight line than were present at any look angle in the $\theta_o = 0°$ case.

When $\theta_o = 40°$, the range of equivalent surface reflectivity changes is increased over the $\theta_o = 20°$ case. The largest scattering angle, 180°, now is found along the longest path length, 40° left. This greatly increases the source function contribution at the left edge of the flight line. An argument similar to that in the preceeding paragraph points to

the fact that we observe the greatest increases in surface reflectivity in the case $\theta_o = 40°$.

Figure 4-8 illustrates the importance of the source function in a different manner. Here, the scattering phase function weighting factor is deliberately minimized by rotation of the plane of observation, and the source function contribution is significantly reduced. Figure 4-8 thus shows a much smaller range of equivalent surface reflectivity changes than does Figure 4-7, its counterpart for principle plane computations.

As stated early in this chapter, an absolute evaluation of the importance of the results in this study cannot be made. Different remote sensing problems will have different accuracy requirements. However, if an investigator were concerned with a problem dealing with natural vegetation surfaces and the atmospheric parameters and aerosol distributions assumed in this study were considered realistic, the numerical results would indeed be meaningful. They could be used as either direct correction factors, or at least employed as an upper limit on atmosphere induced apparent surface reflectivity changes.

Also, consideration of the principles discussed thus far in this chapter leads to several recommendations if it is desired to reduce the atmospheric effect in the remote sensing problem when dealing with surface reflectivities in the range of the natural vegetation type. Measurements should be taken at the lowest practical altitude, particularly if measurements are taken at the shorter wavelengths in the visible portion of the spectrum. The aircraft should be oriented such that the plane of observation is normal to the plane of propagation, thus decreasing the range of scattering angles covered. This geometry also assures symmetry

about $\alpha = 0°$ in both path length and scattering angle. Hence the atmospheric effect is the same for look angles of equal magnitude, and changes in measured intensity for equivalent left and right look angles must be caused by surface variations alone if the atmosphere is horizontally homogeneous. Measurements should be taken as near midday as possible, since equal intensity changes at the smaller solar zenith angle correspond to smaller equivalent surface reflectivity changes.

Finally, this study must close on a note of caution. As Figure 4-9 illustrates, the atmospheric effect changes as surface reflectivity changes due to the interaction between the atmosphere and the surface. Results discussed here should not be extrapolated to the study of surfaces having significantly different reflectivities.

LIST OF REFERENCES

LIST OF REFERENCES

Bullrich, K., "Scattered Radiation in the Atmosphere and the Natural Aerosol," Advances in Geophysics, H. E. Landsberg and J. Van Miegham, Editors, Vol. 10, Academic Press, New York, 1964, pp. 99-260.

Chandrasekhar, S., Radiative Transfer, Clarendon Press, Oxford, 1950.

Coulson, K. L., Dave, J. V., and Sekera, F., Tables Related to Radiation Emerging from a Planetary Atmosphere with Rayleigh Scattering, University of California Press, Berkeley, California, 1960.

Dave, J. V., "Intensity and Polarization of the Radiation Emerging from a Plane-Parallel Atmosphere Containing Monodispersed Aerosols," Appl. Opt. 9, 2673 (1970A).

Dave, J. V., "Coefficients of the Legendre and Fourier Series for the Scattering Functions of Spherical Particles," Appl. Opt. 9, 1888 (1970B).

Dave, J. V., "Development of Programs for Computing Characteristics of Ultraviolet Radiation," Technical Reports 1, 3, 4, and 5, Contract NAS5-21680, NASA, Goddard Space Flight Center, Greenbelt, Maryland, 1972.

Dave, J. V., and Gazdag, J., "A Modified Fourier Transform Method for Multiple Scattering Calculations in a Plane Parallel Mie Atmosphere," Appl. Opt. 9, 1457 (1970).

Deirmendjian, D., Electromagnetics Scattering on Spherical Polydispersions, American Elsevier, New York, 1969.

Handbook of Geophysics, The MacMillan Company, New York, 1960.

Herman, B. M., and Browning, S. R., "A Numerical Solution to the Equation of Radiative Transfer," J. Atmos. Sci. 22, 559 (1965).

van de Hulst, H. C., Light Scattering by Small Particles, John Wiley, New York, 1957.

McClatchey, R. A., Fenn, R. W., Selby, J. E. A., Volz, F. E., and Garing, J. S., Optical Properties of the Atmosphere (Third Edition), AFCRL, Environmental Research Papers, No. 411, AFCRL-72-0497, (1972).

Mie, G., Ann Physik., 25, 377 (1908).

Plass, G. N., and Kattawar, G. W., "Monte Carlo Calculations of Light Scattering from Clouds," Appl. Opt. 7, 415 (1968).

Rayleigh, Lord (J.W. Strutt), Phil. Mag. 41, 107 (1871).

Sekera, Z., "Scattering of Light in the Atmosphere and Diffuse Sky Radiation," Science Progress 179, 479 (1957).